**Jurnal Asiimetrik: Jurnal Ilmiah Rekayasa Dan Inovasi**
Accredited "**SINTA 3**" based on the Decree of Dirjendiktiristek, Number: 225/E/KPT/2022
Volume 7 Number 1, January 2025, Page 83-96
Website : http://journal.univpancasila.ac.id/index.php/asiimetrik/

*p-ISSN 2655-1861*
*e-ISSN 2716-2923*

# The Utilization of Single and Double Orifice Plates in Pipe Inner Flow Structure by Computational Method

## Pemanfaatan Pelat *Orifice* Tunggal dan Ganda pada Struktur Aliran dalam Pipa dengan Metode Komputasi

**Ridwan Daris Naufal[1], James Julian[1*], Fitri Wahyuni[1], Riki Hendra Purba[1], Nely Toding Bunga[2]**
[1]Department of Mechanical Engineering, Faculty of Engineering, Universitas Pembangunan Nasional Veteran Jakarta, Jawa Barat, Indonesia
[2]Department of Mechanical Engineering, Faculty of Engineering, Universitas Pancasila, Jakarta, Indonesia

**Article information:**

Received:
09/12/2024
Revised:
18/12/2024
Accepted:
19/12/2024

**Abstract**

The orifice plate is a device that disrupts the flow in the pipe. The disturbed flow results in the formation of flow structures. The flow structure formed can be utilized for several applications such as multi-fluid mixing and microbubble generator. Using orifice plates to utilize the flow structure results in more significant pressure loss. This study aims to identify the characteristics of the flow structure generated by single and double orifice plates with 1D and 2D spacing at various Reynolds numbers, namely Re = 1×104, 5×104, 1×105, and 5×105, as a basis for application in these various applications. The results show that single and double orifice plates can produce flow structure phenomena such as recirculation and vortex regions. The recirculation area is formed smaller in the double orifice plate due to the flow that is separated faster to converge back to the pipe wall but broader so that the flow of the orifice plate is narrower. Increasing the applied Reynold's number causes the separated flow to reconnect to the pipe wall faster, resulting in a smaller recirculation area. Double orifice plates are more suitable for applications that require a certain degree of mixing or pressure distribution, but with a consequent more significant pressure loss. Meanwhile, single plates can be used for simple needs with little pressure loss.

***Keywords:*** orifice, flow structure, Reynolds Number, recirculation, vortex.

***SDGs*:**


**Abstrak**

Pelat orifice merupakan perangkat yang mengganggu aliran didalam pipa. Aliran yang terganggu mengakibatkan fenomena struktur aliran terbentuk. Struktur aliran yang terbentuk dapat dimanfaatkan untuk beberapa aplikasi seperti pencampuran multi-fluida dan *microbubble* generator. Penggunaan pelat orifice dalam memanfaatkan struktur aliran berdampak pada *pressure loss* yang lebih besar. Oleh karena itu, penelitian ini dilakukan untuk mengetahui karakteristik struktur aliran yang terbentuk dengan pelat orifice tunggal, ganda dengan jarak 1D dan 2D pada variasi bilangan reynold: Re = 1 x 104, 5 x 104, 1 x 105, dan 5 x 105 untuk digunakan pada aplikasi-aplikasi tersebut. Hasilnya menunjukkan bahwa pelat orifice tunggal dan ganda mampu menghasilkan fenomena struktur aliran seperti daerah resirkulasi dan *vortex*. Daerah resirkulasi terbentuk lebih kecil di pelat orifice ganda akibat aliran yang terseparasi lebih cepat untuk menyatu kembali ke dinding pipa, namun lebih lebar sehingga aliran pelat *orifice* lebih sempit. Ditingkatkannya bilangan Reynold yang diaplikasikan menyebabkan aliran yang terseparasi lebih cepat untuk tersambung kembali ke dind-ing pipa, akibatnya daerah resirkulasi lebih kecil. Pelat *orifice* ganda lebih cocok untuk aplikasi yang membutuhkan tingkat pencampuran atau distribusi tekanan tertentu, namun dengan konsekuensi *pressure loss* yang lebih besar. Sementara itu, pelat tunggal dapat digunakan untuk kebutuhan sederhana dengan *pressure loss* yang sedikit.

***Kata Kunci:*** *orifice*, struktur aliran, Bilangan Reynold, resirkulasi, pusaran.

*Correspondence Author
email : zames@upnvj.ac.id

## 1. INTRODUCTION

The Orifice plates are essential in various engineering applications to control fluid flow, improve heat transfer, and create desired turbulence conditions (Bikić *et al.*, 2022). Some direct applications of orifice plates are in industrial piping systems, nuclear power plants, and microbubble generators (Araoye, Badr and Ahmed, 2017; Juwana *et al.*, 2019; Düz, 2021). This application utilizes the flow structure formed due to sudden changes in diameter in the pipe. With this geometric shape, the flow structure on the orifice plate, such as pressure reduction, flow recovery, vena contracta, recirculation areas, and flow vortices, occurs on the downstream side of the orifice plate (Vemulapalli and Venkata, 2022). This flow structure is formed due to the geometry of the orifice plate, where the hole in the orifice plate is smaller than the pipe diameter. However, there is compensation due to the use of the orifice plate in the form of increased pressure loss and power consumption (Bikić *et al.*, 2022). In the industrial sector, an increase in this parameter will be detrimental regarding costs and services. Therefore, further study is needed to improve the performance of the flow structure contained in the orifice plate.

The geometry of the orifice plate determines the flow structure formed in the pipe. Sheikh Nasiruddin and Singh investigated the flow performance of orifice plates with modified geometry (Nasiruddin and Singh, 2021). Modifications are made with curved orifice plates on both the upstream and downstream sides. As a result, a small recirculation area is formed and adjacent to a larger recirculation area immediately downstream of the orifice plate without modification. A small recirculation zone makes the vorticity intensity in the recirculation area even more significant. On the other hand, modifying the orifice plate to the curved shape on the upstream side produces the smallest recirculation area compared to other orifice plate variations. The discharge coefficient value is also more significant than the orifice plate without modification.

Araoye et al. have researched the flow characteristics of double orifice plates (Araoye, Badr and Ahmed, 2017). The research was carried out with a pipe diameter of 25.4 mm with three variations of the hole diameter ratio of an orifice plate (β), each 0.5, 0.63, and 0.77. The range of Reynolds numbers applied is 2.54 x $10^4$ to 1.02 x $10^5$. The results show that when varying β = 0.63 and inlet speed of 2 m/s, adding an orifice plate changes the flow structure in the pipe. Adding an orifice plate creates a new flow area characterized by high-speed flow surrounded by a recirculation area formed between the two plates. A jet-like flow is formed on the double orifice plate with 1D due to the narrowing of the flow due to the recirculation area formed between the two plates.

Several studies have modified the orifice plate design to improve its performance, such as increasing the discharge coefficient, changing the recirculation area, or adjusting the vortices to achieve specific goals. Düz studied pipe flow with an orifice plate with upstream chamfers (Düz, 2021). The chamfer's inclination angle varies based on three angles, namely 15°, 30°, and 45°. Tests were carried out with three variations of the β ratio, namely 0.4; 0.5; and 0.63. In addition, the applied Reynolds number was also varied at 5000, 18400, 91100, and 240000 to determine the impact of different flow conditions. The results show that an orifice plate with a chamfer tilt angle of 30° produces minimal pressure loss of up to 52% compared to an orifice plate without a chamfer. On the other hand, the recirculation zone formed with a chamfer angle of 30° is minimal compared to an orifice plate without a chamfer.

Previous research has investigated the flow structure with several modifications to the orifice plate. Based on previous research, it is known that changes and additions to the geometry of the orifice plate greatly influence the flow structure in the pipe. However, until now, orifice plate modifications have been aimed at reducing the impact of phenomena on the flow structure. On the other hand, the impact of the phenomena that occur on the flow structure can be utilized for several industrial applications, such as multi-fluid mixing or microbubble generators. Therefore, the flow structure formed on the orifice plate needs to be studied comprehensively to develop

knowledge in utilizing and improving this flow structure for industrial applications such as microbubble generators. This study uses a single and double orifice plate with 1D and 2D spacing. Double plate orifice testing is limited to only two plate spacing configurations as they represent practical spacing commonly used in industrial applications such as microbubble generators (Juwana *et al.*, 2019; Đurđević *et al.*, 2019). Adding more orifice plate spacing configurations makes the scope of the study broad without a sufficiently comprehensive understanding of the flow structure changes within the range studied (Araoye, Badr and Ahmed, 2017). The Reynolds number applied is also varied from Re = 1 x $10^4$ to 5 x $10^5$ to determine the impact of several flow conditions. This research used computational methods with validation and verification to obtain data such as flow structure and power consumption following the actual conditions.

## 2. METHODOLOGY

This research used the numerical computation method of ANSYS Fluent as a third-party software for internal fluid flow simulation. This method is carried out by undergoing three main steps: pre-processing, processing, and post-processing (Julian, Anggara and Wahyuni, 2024). Pre-processing is done by creating the required geometry, meshing, and determining boundary conditions. After that, the processing step is performed, and the results are tested for data feasibility through mesh independence test and validation (Julian, Iskandar and Wahyuni, 2022). The results of the data feasibility test determine whether the data is suitable for further analysis. That way, conclusions can be drawn from the results of the data that has been analyzed.

### 2.1. Flow Structures of Orifice Plates

The phenomena formed through the orifice plate flow can be used for industrial applications such as multi-phase fluid mixing and microbubble generators (Ahmed *et al.*, 2023). The recirculation area and vortex formed on the downstream side of the orifice plate create a vacuum and rotating pressure area (Julian, Anggara and Wahyuni, 2024). The recirculation zone formation and vortex are influenced by several factors, including the working fluid properties, the geometry design of the orifice plate, and the addition of the orifice plate (Abed *et al.*, 2020). Flow structures such as recirculation and vortex area patterns can be seen visually with streamlined visualization, as shown in Figure 1. The length of the recirculation area can be determined by the position of the separation point and the position of the reattachment point, which is obtained from the coefficient of friction on the pipe wall (Julian, Iskandar and Wahyuni, 2023). In general, the coefficient of friction is obtained with the Equation 1.

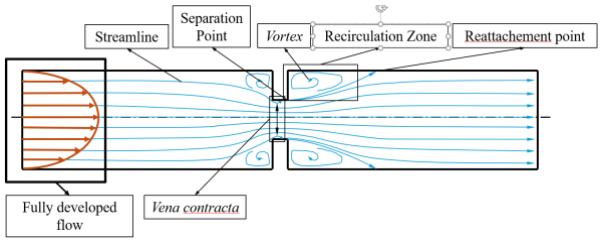


**Figure 1.** Visualization of the flow structure on the ori-fice plate (Shaaban, 2014; Düz, 2021).

$$C_f = \frac{\tau_w}{\frac{1}{2}\rho u^2} \quad (1)$$

where:

$C_f$ = Coefficient of Friction

$\tau_w$ = wall shear stress (Pa)

$\rho$ = Fluid density (kg/$m^3$)

u = Fluid Velocity (m/s)

### 2.2. Numerical Method

#### *2.2.1. Numerical Method*

The geometry of the single-orifice and double-plate orifice designs is shown in Fig-ures 2, 3, and 4. To save computational re-quirements, the fluid domain in this study uses Two-Dimensional shapes (Julian, Iskandar, Wahyuni and Ferdyanto, 2022). This study uses pipe geometry with dimensions according to industry standards such as microbubble generators, namely pipe diameter $D$ = 70.3 mm and the ratio of orifice plate diameter to pipe diameter $\beta$ = 0.7 to analyze the flow structure formed (Juwana *et al.*, 2019; Đurđević *et al.*, 2019; Collins and Clark, 2022).

The selection of pipe diameter and $\beta$ ratio is still within the range of ISO 5167-2:2003 standard for using orifice plates. The test requires a fully developed flow on the upstream and downstream sides of the orifice plate (Shah *et al.*, 2012). The length of the pipe on the upstream side is made as long as 12D and downstream along 33D, with the total length of the pipe made (L) being 3.167 x $10^3$ mm to ensure a fully developed flow. The tested orifice plate has a thickness (t) of 3.5mm. Therefore, this study's single orifice plate geometry has met the ISO 5167-2:2003 standard (see Figure 2).

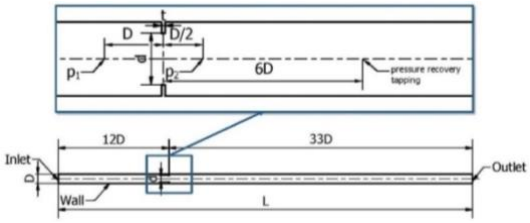


**Figure 2.** Single orifice plate geometry design and boundary condition.

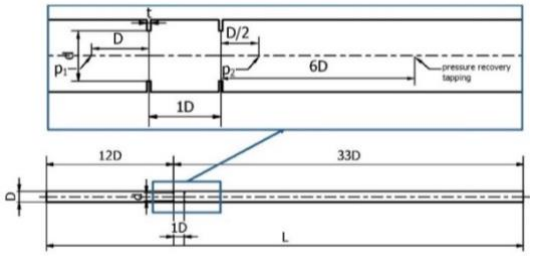


**Figure 3.** Double orifice plate with 1D spacing geometry design.

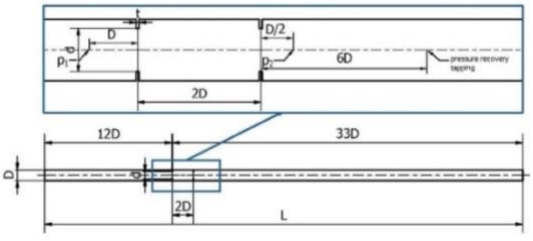


**Figure 4.** Double orifice plate with 2D spacing geometry design.

Three orifice plate geometries are simu-lated in this study: single plate orifice, double orifice plate with 1D distance from the first orifice (see Figure 3), and double plate orifice plate with 2D distance from the first orifice (see Figure 4). The addition of the orifice plate is adapted to the ISO 5167 - 2:2003 standard because there is no standard governing the addition of the orifice plate. Three orifice plate shapes are simulated with four variations of a wide range of Reynold numbers: Re = 1 x $10^4$, 5 x $10^4$, 1 x $10^5$, and 5 x $10^5$. This range of variation allows a comprehensive analysis of the formation of flow structures, such as recirculation zones and vortex patterns, until the pressure distribution changes with increasing Reynolds number. On the other hand, flow conditions in the Reynolds num-ber range tested in this study are also com-monly used in industrial applications such as microbubble generators (Xie and Xi, 2017).

Inlet velocity on the upstream side is applied to this simulation based on the var-ied Reynold's number. The type of fluid used in this study is water with a constant density at ρ = 998.2 kg/$m^3$ to obtain varying inlet velocities. In addition, the wall is set as a no-slip condition, and the outlet side downstream of the pipe is set with outflow to eliminate the zero-pressure effect (Araoye, Badr and Ahmed, 2017).

### *2.2.2. Meshing*

Meshing is one of the processes in numerical computing that divides the geom-etry domain into small elements to facilitate numerical calculations. These arranged small parts are also called mesh elements. For two-dimensional fluid domains, there are several forms of mesh available. The simulation conducted in this study uses a structured type of mesh with a quadrilateral shape, shown in **Figure 5**.

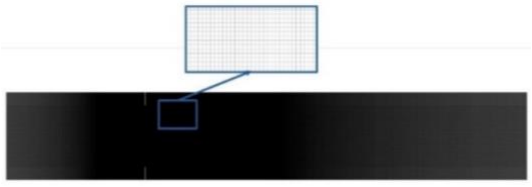

**Figure 5.** Quadrilateral shape in the mesh process of orifice plate simulation.

This shape has several advantages, including a cheaper computational cost per iteration than other mesh shapes (Julian *et al.*, 2024). In addition, this mesh shape is more accessible for creating simple geometries than other mesh shapes (Julian, Iskandar, Wahyuni, Armansyah, *et al.*, 2022).

*2.2.3. Governing Equation*

The numerical computation process to simulate the orifice plate uses the RANS governing equations. These equations in-clude the continuity equation, which de-scribes the conservation of mass and mo-mentum which shows the conservation of momentum (Julian, Iskandar and Wahyuni, 2023). These equations are shown in 6 and 7, respectively (Julian, Anggara and Wahyuni, 2023). In addition, turbulent models are required to predict complicated turbulent fluid flows. Various turbulent models are available in the numerical computing pro-cess. This research uses a k-ε type turbulent model because the coefficients governing the turbulent model are suitable for use at low to medium Reynold numbers (Julian *et al.*, 2023). The k-ω turbulent model equation is shown in equation 8, which describes the turbulent kinetic energy equation, and equation 9, which shows the energy dissipation rate (Julian, Iskandar, Wahyuni and Ferdyanto, 2022). Thus, the turbulent model complements the RANS equation for numerical computation.

$$\frac{\partial \rho}{\partial t}+\frac{\partial}{\partial x_i}(\rho u_i)=0 \tag{6}$$

$$\frac{\partial}{\partial t}(\rho u_i)+\frac{\partial}{\partial x_i}(\rho u_i u_j)=\frac{\partial p}{\partial x_i}+\frac{\partial}{\partial x_j}\left[\mu\left(\frac{\partial u_i}{\partial x_j}+\frac{\partial u_j}{\partial x_i}-\frac{2}{3}\delta_{ij}\frac{\partial u_i}{\partial x_i}\right)\right]+\frac{\partial}{\partial x_i}\left(-\rho\overline{u_i' u_j'}\right) \tag{7}$$

$$\frac{\partial k}{\partial t}+U_j\frac{\partial k}{\partial x_j}=\tau_{ij}\frac{\partial U_i}{\partial x_j}-\beta^* k\omega+\frac{\partial}{\partial x_j}\left[\left(v+\sigma^* v_T\right)\frac{\partial k}{\partial x_j}\right] \tag{8}$$

$$\frac{\partial \omega}{\partial t}+U_j\frac{\partial \omega}{\partial x_j}=\alpha\frac{\omega}{k}\tau_{ij}\frac{\partial U_i}{\partial x_j}-\beta\omega^2+\frac{\partial}{\partial x_j}\left[\left(v+\sigma v_T\right)\frac{\partial \omega}{\partial x_j}\right] \tag{9}$$

where:

$\alpha=\frac{5}{9}$, $\beta=\frac{3}{40}$, $\beta^*=\frac{9}{100}$, $\sigma=\frac{1}{2}$, $\sigma^*=\frac{1}{2}$,

$\varepsilon=\beta^*\omega k$

*2.2.4. Mesh Independence Test*

The mesh independence test is conducted as a verification process in this re-search. In this process, the mesh quality is evaluated based on the discretization error to determine the mesh used (Julian *et al.*, 2023). This research applies the Richardson Roache ex-trapolation method to perform mesh inde-pendence tests. A fine mesh with 1.3165 x $10^6$ elements was selected to provide high-resolution simulation results, especially in the pressure tapping and flow structure ar-eas formed. Medium mesh with 6.5825 x $10^5$ element and coarse mesh with 3.2950 x $10^5$ were added to compare the results, as well as ensure the stability and consistency of the simulation at any resolution change with an element ratio of 5 (Bikić *et al.*, 2022).

$$r=\frac{h_2}{h_1} \tag{10}$$

$$\bar{p}=\frac{\ln\left(\frac{f_3-f_2}{f_2-f_1}\right)}{\ln(r)} \tag{11}$$

$$GCI_{fine}=\frac{F_s\,|\in|}{\left(r^{\bar{p}}-1\right)} \tag{12}$$

$$GCI_{coarse}=\frac{F_s\,|\in|\,r^{\bar{p}}}{\left(r^{\bar{p}}-1\right)} \tag{13}$$

$$\in=\frac{f_{n+1}-f_n}{f_n} \tag{14}$$

$$\frac{GCI_{fine}}{GCI_{coarse}\,r^{\bar{p}}}\approx 1 \tag{15}$$

$$f r_{h=0}=f_1+\frac{(f_1-f_2)}{\left(r^{\bar{p}}-1\right)} \tag{16}$$

where:

r = Ratio between two grid sizes (dimensionless)

$\overline{p}$ = Convergence Order (dimensionless)

$GCI_{fine}$ = Grid Convergence Index for fine mesh (dimensionless)

$f\,r_{h=0}$ = Reference Solution for zero refinement (°)

The ratio between mesh is determined by equation 10. The parameter for the mesh independence test is the pressure at point p1, in the middle of the pipe 1D upstream side of the orifice plate. After that, the Or-der for the mesh independence test is cal-culated by equation 11. Mesh convergence index for fine and coarse mesh is obtained using equations 12 and 13, respectively. The mesh independence test results are ob-tained by considering the convergent range around ~1, calculated by equation 15. Thus, the error can be calculated using Equation 16. Referring to some previous studies using the Richardson extrapolation method, the mesh type that can be used for further testing is below one percent with the slightest error (Iskandar *et al.*, 2022; Julian *et al.*, 2023; Lukiano *et al.*, 2023). It can be con-cluded that the fine mesh with the number of elements 1.3165 x $10^6$ is used in this study. Table 1 showing the results of the mesh independence test.

**Table 1.** Mesh independence test result.

| Parameter | Fine | Medium | Coarse |
|---|---|---|---|
| $p$ | 20358,37 | 20396,37 | 20693,14 |
| $\overline{\overline{p}}$ | | 1,28 | |
| $r$ | | 5 | |
| $GCI_{fine}$ | | 0,03% | |
| $GCI_{coarse}$ | | 0,27% | |
| $\frac{GCI_{coarse}}{GCI_{fine}r^{\overline{\overline{p}}}}$ | | 1,00 | |
| *Error* | 0,03% | 0,21% | 1,67% |

## 3. RESULTS AND DISCUSSION

### 3.1. Validation

In this research, validation is carried out to ensure that the simulation data follows the actual conditions. The $C_O$ value from the single orifice simulation with betta = 0.7 was validated with data from the ISO-5167-2:2003 standard. The results are shown in Figure 6. The average error value between the two data is 0.10%, with a maximum deviation of 0.43%. In addition, the trend of changes in the value of each simulation result looks similar. Based on the validation results, it can be said that the simulation is valid against the ISO-5167:2 2003 standard.

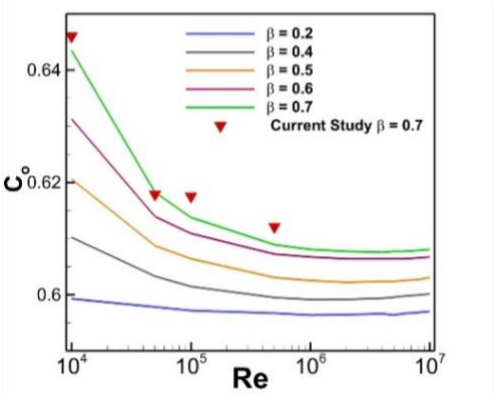


**Figure 6.** Relationship graph of orifice plate discharge coefficient ($C_O$) and Reynold number (Re) for validation with ISO 5167-2:2003

### 3.2. Analysis

Figure 7 shows the velocity profile and x-velocity contours along the pipe with the orifice plate variation. The figure shows that every flow entering the orifice plate has formed a velocity gradient. The closer the fluid is to the pipe wall, the smaller the flow velocity until it is zero right at the wall. The velocity profile shows that the flow formed before and after entering the orifice plate is fully developed. Therefore, the flow test on the orifice plate has met the requirements, as Shah et al. referred to (Shah *et al.*, 2012).

Figure 7 shows that the flow velocity increases as it enters the orifice plate due to the narrowed geometry. Downstream, a recirculation region forms as the flow near the wall moves opposite the main flow. The velocity profile recovers at a certain distance downstream for a single orifice plate, as shown in Figure 7 (a). However, the second plate disrupts the flow in double orifice plates, causing re-separation and forming another recirculation region downstream, as shown in Figure 7 (b) and (c). The addition of the second plate extends the recirculation area, with spacing also affecting its length. As shown in Figure 7 (c), a 2D spacing results in a more extended recirculation area.

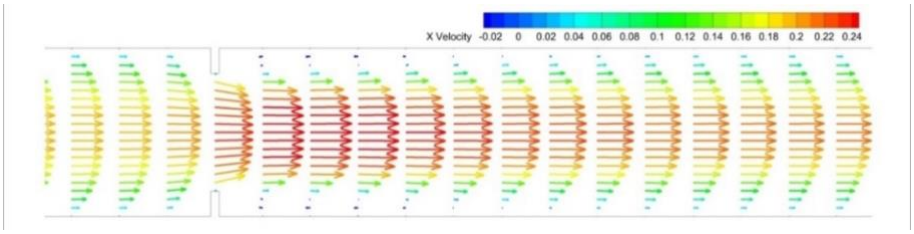


(a) Single orifice plate

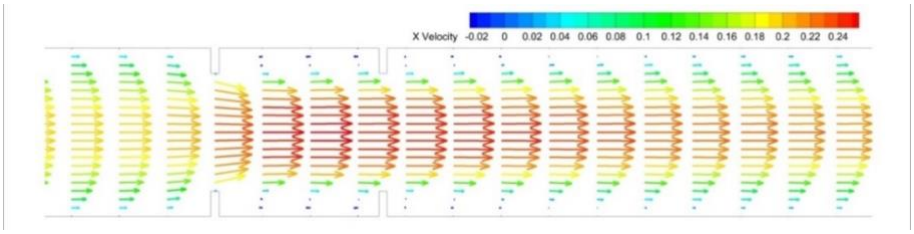


(b) Double orifice plate with 1D spacing

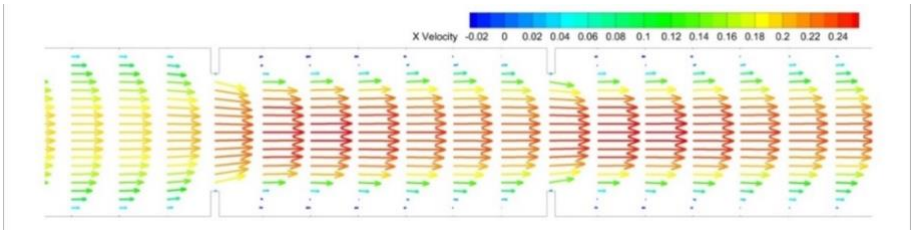


(c) Double orifice plate with 2D spacing

**Figure 7.** Velocity Profile and Contour along the pipe on orifice plate variation with Reynolds Number Re = 1 x $10^4$.

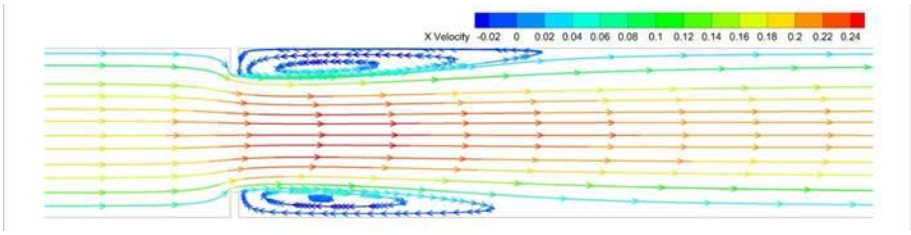


(a) Single Orifice Plate

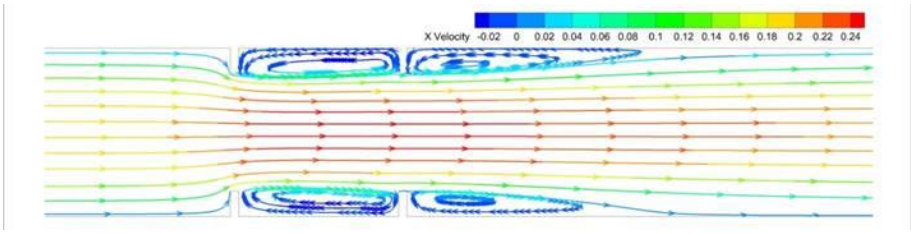


(b) Double Orifice Plate with 1D spacing

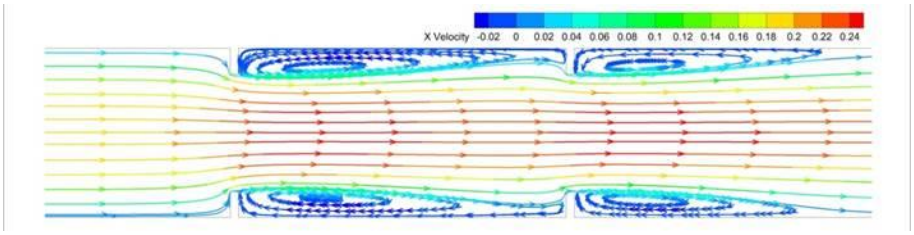


(c) Double Orifice Plate with 2D spacing

**Figure 8.** Streamline along the pipe on orifice plate variation with Reynolds Number Re = 1 x $10^4$.

Figure 8 show the streamlined visualization on single, double with 1D spacing, and double with 2D spacing orifice plates at Reynold's number Re = 1 x $10^4$. Figure 8 (a) shows that on a single orifice plate, a vortex inside the recirculation zone is formed on the downstream side of the orifice plate. This finding is consistent with Araoye et al., research that the vortex is formed due to the difference in flow direction and velocity around the recirculation area (Araoye, Badr and Ahmed, 2017).

In Figure 8 (b), the addition of orifice plates spaced 1D apart at a Reynolds number of Re = 1 x $10^4$ results in two recirculation zones forming on each downstream side of the plates. The first recirculation zone forms behind the first orifice plate and fills the area between the two plates, while the second zone appears on the downstream side of the second plate. This configuration also forms the vortex twice. When the distance between the plates is increased to 2D, as shown in Figure 8 (c), the recirculation zone expands between the two plates, forming one more enormous primary vortex. In addition, the flow passing through the second plate becomes narrower due to the flow not fully recovering after passing through the first plate, so it experiences reseparation at the second plate, further narrowing the flow and increasing the fluid velocity. Thus, following the results of research Araoye et al. (Araoye, Badr and Ahmed, 2017), the addition of orifice plates increases the recirculation area formed, and changes in distance affect the characteristics of the flow formed.

Figure 9 shows a graph of the distribution of skin friction coefficient (Cf) along the pipe. The Cf graph shows a similar pattern for single and double orifice plate configurations on the upstream side of the orifice plate because the pipe geometry is still the same. The Cf value decreases until zero when the flow experiences separation before entering the orifice plate hole (Julian, Iskandar, Wahyuni and Ferdyanto, 2022). On the downstream side of the single orifice plate, the Cf value again increases until it approaches a value similar to the upstream side. This pattern shows that the recirculation zone on the downstream side of the orifice plate has a maximum Cf value that is almost the same as the upstream side.

The Cf trend in the double orifice plate configuration shows a second and third peak due to flow separation and reattaches. The second peak has a smaller maximum value than the first peak. In the double orifice plate configuration with 2D spacing, a second small peak is formed between the two plates. It is consistent with the streamline, which shows two recirculation zones with smaller sizes and intensities in the second recirculation zone.

The length of the recirculation area is determined by the distance between the points where the fluid boundary layer separates and reattaches along the pipe. The Cf distribution graph can identify the reattachment point when the value reaches zero (Julian, Iskandar, Wahyuni and Ferdyanto, 2022). Figure 10 shows that a single orifice plate results in a more extended recirculation area of up to 1.93D, compared to a double orifice plate with a 1D spacing of 1.57D and 2D spacing of 1.62D. It supports the double orifice plate study conducted by Araoye et al. (Araoye, Badr and Ahmed, 2017) that adding orifice plates accelerates reattachment and thus shortens the recirculation area. However, increasing the distance between plates causes the recirculation area to lengthen again.

Increasing the Reynolds number shortens the reattachment length. At Re = 1 x $10^4$, the reattachment length downstream of the single orifice plate is 1.93D, further when the Reynolds number is increased to Re = 5 x $10^4$, the reattachment length is reduced by about 29.41% to 1.36D, and there is another reduction of about 33.45% to 1.29D at Re = 5 x $10^5$. In agreement with previous research, reattachment length decreases because turbulent flows at high Reynolds numbers have more significant momentum and energy, allowing them to reattach more quickly (Abed *et al.*, 2020).

The vortex formed in the recirculation zone creates a low-pressure region, as shown in the pressure contours in Figure 10. Low pressure is formed on the downstream side of the orifice plate due to the recirculation zone's vortex. In the double orifice plate configuration with 2D spacing, the vacuum region on the downstream

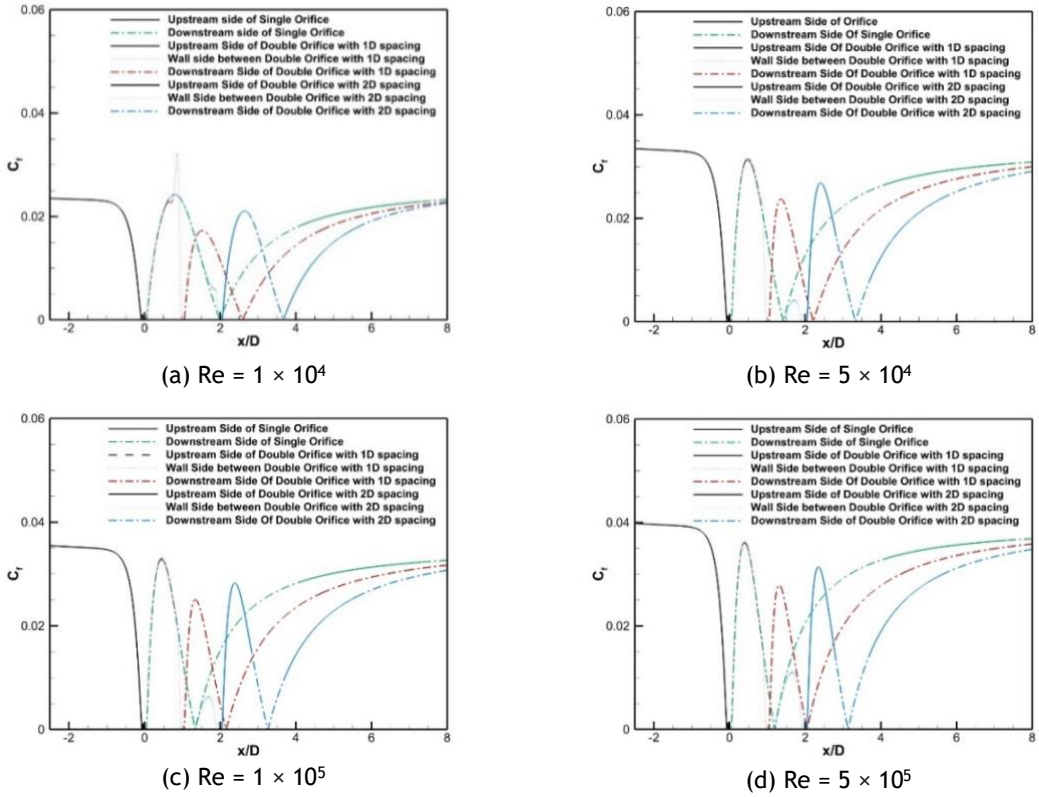


(a) Re = 1 × $10^4$ (b) Re = 5 × $10^4$

(c) Re = 1 × $10^5$ (d) Re = 5 × $10^5$

**Figure 9.** $C_f$ curve distribution on the pipe wall.

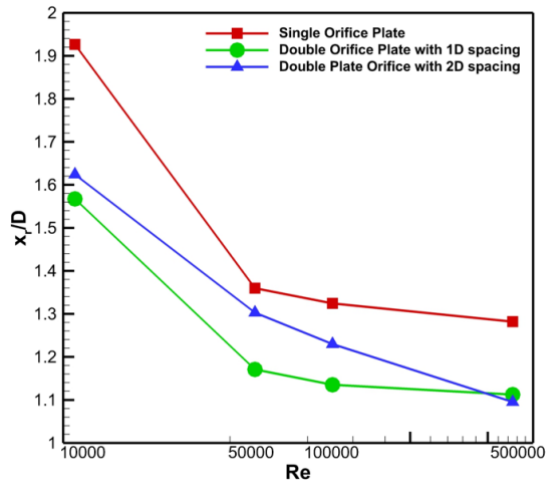


**Figure 10.** Recirculation zone length ($x_r$) on the down-stream side of the single orifice plate and the second orifice plate in the double configuration.

side of the second plate becomes more intense than in the other configurations. It is suggested that adding 2D-spaced orifice plates can generate lower pressure, which, according to Juwana et al. research (Juwana *et al.*, 2019), can be utilized in applications such as microbubble generators.

From the perspective of pressure distribution along the pipe centerline, as shown in Figure 11, a sudden pressure drop occurs at each orifice plate variation due to disturbed flow. At Re = 1 x 104, the double orifice plate with a 1D spacing slightly delays pressure recovery, increasing pressure loss by about 15%. When the spacing is increased to 2D, the minimum pressure point shifts towards the second orifice plate due to the narrowing flow caused by the orifice and its


(a) Single orifice plate


(b) Double orifice plate with 1D spacing

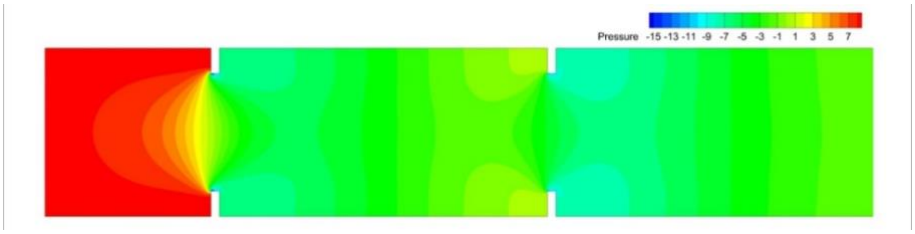


(c) Double orifice plate with 2D spacing

**Figure 11.** Pressure contour along the pipe on the Orifice Plate Variation with Reynolds Number Re = 1 x $10^4$.

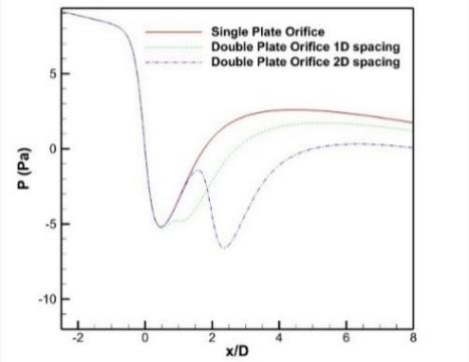


(a) Re = 1 × $10^4$

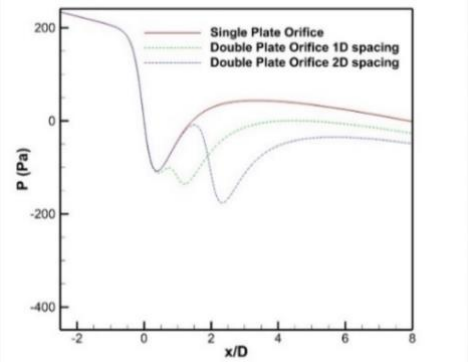


(b) Re = 5 × $10^4$

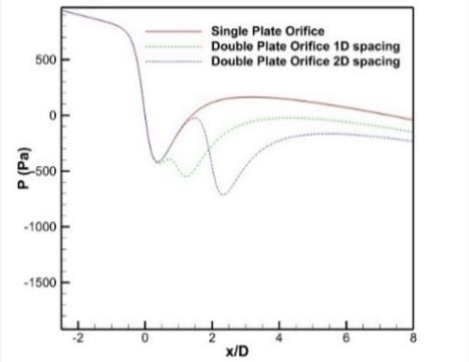


(c) Re = 1 × $10^5$

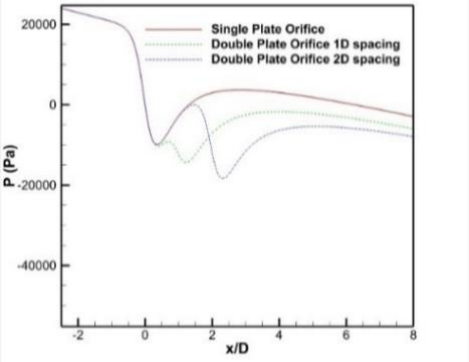


(d) Re = 5 × $10^5$

**Figure 12.** Centerline axial pressure distribution.

recirculation zone. This constriction forms a vena contracta, where the pressure drops to its minimum and velocity peaks (Shan *et al.*, 2016).

The vena contracta occurs as the flow narrows beyond the orifice hole due to the recirculation zone extending past the diameter. At Re ≥ $5\times10^4$, the pressure distribution shows a similar pattern, with the vena contracta shifting to the second orifice plate at 1D and 2D distances (see Figure 12). However, the pressure drop is more significant with a 2D spacing, and multiple orifice plates make pressure recovery more difficult, increasing overall pressure loss. According to research by Juwana et al., the increase in pressure loss is a consequence of utilizing the flow structure formed for the microbubble generator (Juwana *et al.*, 2019). However, this may increase power usage in using orifice plates to disrupt the flow (Bikić *et al.*, 2022).

## 4. CONCLUSION

Research using single and double ori-fice plates in flow structures has been con-ducted using numerical computing meth-ods. Tests were carried out with four varia-tions in the Reynolds number on three dif-ferent orifice plate constructions, including single orifice plates, double orifice plates with 1D spacing, and orifice plates with 2D spacing. The results show that the flow on the orifice plate forms several flow structure phenomena, such as boundary layer separa-tion, recirculation areas, and vortexes. The recirculation zone in the double orifice plate is shorter but broader, especially in the 2D spacing configuration, as the flow has time to recover before re-separation at the second plate. Increasing the Reynolds number results in a smaller recirculation zone due to faster flow converging back to the pipe wall.

The vortex-like flow structure formed within the recirculation zone creates a vac-uum pressure zone downstream of the ori-fice plate. The vacuum pressure formed in the double orifice plate with 2D spacing is better than the single or double orifice plate configuration with 1D spacing. It is very necessary in the formation of mi-crobubbles in the microbubble generator. In other words, double orifice plates with 2D spacing are suitable for microbubble gener-ators.

On the other hand, using orifice plates, whether single or multiple, leads to pressure losses that directly impact the energy loss. Therefore, selecting the proper orifice plate configuration is critical to utilizing the de-sired flow structure. From a design perspec-tive, double orifice plates are more suitable for applications that require specific mixing or pressure distribution, albeit at the ex-pense of energy efficiency. Meanwhile, sin-gle plates are more efficient for simple needs, prioritizing energy savings as they have minimal pressure loss. Thus, this re-search provides essential insights into pip-ing system design and orifice plate optimi-zation with the help of computational simu-lation, which enables in-depth analysis of flow patterns and power consumption be-fore implementation.

## REFERENCES

Abed, N. *et al.* (2020) 'Experimental And Numerical Investigations For Turbulent Air Flow Characteristics Of Circular Orifice Plate', *IOP Conference Series: Materials Science and Engineering*, 881(1), p. 012050. Available at: https://doi.org/10.1088/1757-899X/881/1/012050.

Ahmed, S. *et al.* (2023) 'Design Modification In An Industrial Multistage Orifice To Avoid Cavitation Using CFD Simulation', *Journal of the Taiwan Institute of Chemical Engineers*, 148, p. 104833. Available at: https://doi.org/10.1016/j.jtice.2023.104833.

Araoye, A.A., Badr, H.M. and Ahmed, W.H. (2017) 'Investigation Of Flow Through Multi-Stage Restricting Orifices', *Annals of Nuclear Energy*, 104, pp. 75–90. Available at: https://doi.org/10.1016/j.anucene.2017.02.002.

Bikić, S. *et al.* (2022) 'Comparison Of Single-Hole And Multi-Hole Orifice Energy Consumption', *Advances in Mechanical Engineering*, 14(1), pp. 1–13. Available at: https://doi.org/10.1177/16878140221075461.

Collins, A. and Clark, S. (2022) 'Additional Data Supporting The 2022 Updates To The ISO 5167 Standards', *Flow Measurement and Instrumentation*, 86, p. 102193. Available at: https://doi.org/10.1016/j.flowmeasinst.2022.102193.

Đurđević, M. *et al*. (2019) 'Experimental Research Of Single-Hole And Multi-Hole Orifice Gas Flow Meters', *Flow Measurement and Instrumentation*, 70, p. 101650. Available at: https://doi.org/10.1016/j.flowmeasinst.2019.101650.

Düz, H. (2021) 'Effect Of Conical Angle On The Hydraulic Properties Of Orifice Plate Flows: A Numerical Approach', *Flow Measurement and Instrumentation*, 81, p. 102026. Available at: https://doi.org/10.1016/j.flowmeasinst.2021.102026.

Iskandar, W. *et al*. (2022) 'Study of Airfoil Characteristics on NACA 4415 with Reynolds Number Variations', *International Review on Modelling and Simulations (IREMOS)*, 15(3), pp. 162–171. Available at: https://doi.org/10.15866/iremos.v15i3.21684.

Julian, J., Iskandar, W., Wahyuni, F. and Ferdyanto, F. (2022) 'Computational Fluid Dynamics Analysis Based On The Fluid Flow Separation Point On The Upper Side Of The NACA 0015 Air-foil With The Coefficient of Friction', *Media Mesin: Majalah Teknik Mesin*, 23(2), pp. 70–82. Available at: https://doi.org/10.23917/mesin.v23i2.18217.

Julian, J., Iskandar, W., Wahyuni, F., Armansyah, A., *et al*. (2022) 'Effect of Single Slat and Double Slat on Aerodynamic Performance of NACA 4415', *International Journal of Marine Engineering Innovation and Research*, 7(2), pp. 93–100. Available at: https://doi.org/10.12962/j25481479.v7i2.12875.

Julian, J. *et al*. (2023) 'The Effect of Micro Geometry with Various Forms as Passive Flow Control in NACA 4415', *Jurnal Asiimetrik: Jurnal Ilmiah Rekayasa & Inovasi*, 5(2), pp. 231–242. Available at: https://doi.org/10.35814/asiimetrik.v5i2.4678.

Julian, J. *et al*. (2024) 'Numerical Analysis of Gurney Flap Impact on NACA 4415 Airfoil Aerodynamics Performance', *Jurnal Asiimetrik: Jurnal Ilmiah Rekayasa & Inovasi*, 6(1), pp. 121–132. Available at: https://doi.org/10.35814/asiimetrik.v6i1.5722.

Julian, J., Anggara, R.A. and Wahyuni, F. (2023) 'Influence of Slat Size Variation as Passive Flow Control Instruments on NACA 4415 Airfoil Toward Aerodynamic Performance', *International Journal of Marine Engineering Innovation and Research*, 8(2), pp. 367–375. Available at: https://doi.org/10.12962/j25481479.v8i2.16427.

Julian, J., Anggara, R.A. and Wahyuni, F. (2024) 'Numerical Study On Characteristics Of The Backward-Facing Step Flow With Variations Of The Slope Angle Of The Step', *Jurnal Polimesin*, 22(1), pp. 6–14. Available at: https://doi.org/10.30811/jpl.v22i1.4052.

Julian, J., Iskandar, W. and Wahyuni, F. (2022) 'Aerodynamics Improvement of NACA 0015 by Using Co-Flow Jet', *International Journal of Marine Engineering Innovation and Research*, 7(4), pp. 284–291. Available at: https://doi.org/10.12962/j25481479.v7i4.14898.

Julian, J., Iskandar, W. and Wahyuni, F. (2023) 'Leading Edge Modification of NACA 0015 and NACA 4415 Inspired by Beluga Whale', *International Journal of Marine Engineering Innovation and Research*, 8(2), pp. 222–231. Available at: https://doi.org/10.12962/j25481479.v8i2.16432.

Juwana, W.E. *et al*. (2019) 'Hydrodynamic Characteristics Of The Microbubble Dissolution In Liquid Using Orifice Type Microbubble Generator', *Chemical Engineering Research and Design*, 141, pp. 436–448. Available at: https://doi.org/10.1016/j.cherd.2018.11.017.

Lukiano, M.F. *et al*. (2023) 'The Influence of Mounting Angle on Gurney Flap on The Aerodynamics Performance of NACA 0015 Using CFD Method', *International Journal of Marine Engineering Innovation and Research*, 8(4), pp. 694–702. Available at: https://doi.org/10.12962/j25481479.v8i4.18891.

Nasiruddin, S. and Singh, S.N. (2021) 'Performance Evaluation Of An Innovative Design Modification Of An Orifice Meter', *Flow Measurement and Instrumentation*, 80, p. 101944. Available at: https://doi.org/10.1016/j.flowmeasinst.2021.101944.

Shaaban, S. (2014) 'Optimization Of Orifice Meter's Energy Consumption', *Chemical Engineering Research and Design*, 92(6), pp. 1005–1015. Available at: https://doi.org/10.1016/j.cherd.2013.08.022.

Shah, M.S. *et al*. (2012) 'Analysis Of Flow Through An Orifice Meter: CFD Simulation', *Chemical Engineering Science*, 71, pp. 300–309. Available at: https://doi.org/10.1016/j.ces.2011.11.022.

Shan, F. *et al*. (2016) 'Effects Of The Orifice To Pipe Diameter Ratio On Orifice Flows', *Chemical Engineering Science*, 152, pp. 497–506. Available at: https://doi.org/10.1016/j.ces.2016.06.050.

Vemulapalli, S. and Venkata, S.K. (2022) 'Parametric Analysis Of Orifice Plates On Measurement Of Flow: A Review', *Ain Shams Engineering Journal*, 13(3), p. 101639. Available at: https://doi.org/10.1016/j.asej.2021.11.008.

Xie, W.A. and Xi, G.N. (2017) 'Fluid Flow And Heat Transfer Characteristics Of Separation And Reattachment Flow Over A Backward-Facing Step', *International Journal of Refrigeration*, 74, pp. 177–189. Available at: https://doi.org/10.1016/j.ijrefrig.2016.10.006.